Light Metals 2012 *Edited by: Carlos E. Suarez*
TMS (The Minerals, Metals & Materials Society), 2012

BALL-MILLED Cu-Ni-Fe-O MATERIALS AS INERT ANODES FOR ALUMINUM ELECTROLYSIS IN LOW-TEMPERATURE KF-AlF_3 ELECTROLYTE

S. Helle[1], B. Davis[2], D. Guay[1], L. Roué[1]
[1]INRS-Énergie Matériaux Télécommunication; 1650 Boulevard Lionel-Boulet; Varennes, Québec, J3X 1S2, Canada
[2]Kingston Process Metallurgy Inc.; 1079 Pembridge Crescent; Kingston, Ontario, K7P 1P2, Canada

Keywords: aluminum electrolysis, inert anode, Cu-Ni-Fe-O alloys, mechanical alloying, low-temperature electrolyte

Abstract

A series of compounds with the general formula $(Cu_{65}Ni_{20}Fe_{15})_{97.7}O_{2.3}$ were prepared by high energy ball milling and evaluated as inert anodes for aluminum electrolysis at 700°C. All compounds had the same nominal composition but O_2 was introduced at different moments during the milling operation. All compounds show the presence of an fcc phase (γ-phase). Upon heat-treatment at 1000°C during the subsequent powder consolidation, the added O reacts with Fe to form more or less well dispersed Fe_2O_3 precipitates. Dry oxidation tests at 700°C showed that the material oxidation behavior strongly depended on the moment when O_2 is added. The best results were obtained when O_2 is added after the γ-phase is formed. The use of this anode for Al electrolysis in low-temperature (700°C) KF-AlF3 electrolyte for 20 h showed that the cell voltage is stable at ca. 4.2 V and the Cu contamination of the produced Al is 0.2 wt.%. In this case, the size, dispersion and concentration of Fe_2O_3 precipitates in the consolidated powder are optimized to promote the formation of a protective $NiFe_2O_4$ layer on the anode surface.

Introduction

Cu-Ni-Fe alloys are promising candidates as inert anodes for low-temperature Al electrolysis **[1,2]**. However, Cu-Ni-Fe alloys present a two-phased microstructure (a Cu-rich phase and a Fe-Ni-rich phase) over a large composition range **[3]**. This chemical inhomogeneity has a negative impact on their corrosion resistance because the iron-rich phase is preferentially corroded during Al electrolysis. This induces the formation of iron fluoride corrosion tunnels in the anode scale as recently shown by Beck et al. **[4]**. This limitation can be partially circumvented by careful homogenization of the alloy through an appropriate thermal treatment **[4,5]**.

Highly homogeneous Cu-Ni-Fe alloys can be synthesized by mechanical alloying **[6-8]**. It was shown that the Cu content in mechanically alloyed $Cu_xNi_{85-x}Fe_{15}$ must be higher than 60 wt.% to obtain an anode giving a constant cell potential and maintaining its mechanical integrity during aluminum electrolysis for 20 h in low-temperature (700 °C) KF-AlF_3 electrolyte. However, for a Cu content > 70 wt.%, the dissolution rate of the anode increases dramatically. Actually, the optimal Cu content in $Cu_xNi_{85-x}Fe_{15}$ is restricted to a narrow range around 65-70 wt.%. In this composition range, the formation of a dense Cu_2O-rich external layer on the electrode surface with an inner $NiFe_2O_4$-rich scale is favoured during Al electrolysis, leading to a good corrosion resistance of the anode **[7]**. In addition, as the Fe content of the Cu-Ni-Fe alloy is increased, the $NiFe_2O_4$ content of the internal layer is also increased, resulting in a better stabilisation of the cell voltage **[8]**. However, increasing the Fe concentration in the alloy increases also the Fe content in the produced Al. Thus, a Fe concentration of 15 wt.% appears as the most appropriate value, leading to the production of Al with a purity exceeding 99.3 wt.%.

The corrosion resistance of the mechanically alloyed $Cu_{65}Ni_{20}Fe_{15}$ anode still needs to be improved for long-term use in Al electrolysis cells and to be able to produce aluminum meeting the purity specification of most commercial Al (purity ≥ 99.7%).

In the present study, Cu-Ni-Fe-O materials are prepared by mechanical alloying under oxygen atmosphere. Their structural and chemical characteristics are studied at different stages of their preparation and after 20 h of electrolysis in low-temperature (700°C) KF-AlF_3 electrolyte. It will be shown that oxygen added during the mechanical alloying process has a beneficial effect on the electrode corrosion resistance.

Experimental

The Cu-Ni-Fe-O materials were synthesized by high energy ball milling (HEBM) according to the schema presented in **Fig. 1**. The samples were designated as follows: S0-10, S1-9, S5-5, S10-0 and S10-5. The first number corresponds to the milling time under Ar and the second one is the milling time under O_2. In a first step, elemental Cu, Ni and Fe powders in the proportion 65:20:15 (wt.%) were milled under Ar atmosphere for a duration ranging from 0 to 10 h. Stearic acid (0.5 wt.%) was also added in order to prevent excessive cold welding. Milling in presence of O_2 was performed by periodically opening the vial in a pure O_2 atmosphere (pressure of 1 atm) to replenish it. The total milling time was fixed at 10 h except for one sample milled for 15 h. The milling was performed using a vibratory miller (SPEX 8000M). The ball-to-powder mass ratio (BPR) was 2:1. The oxygen content (measured with a LECO oxygen analyser) in the different samples milled under O_2 was 2.3 wt.% compared to 0.3 wt.% for the sample only milled under argon. The Cu, Ni and Fe concentrations measured by energy dispersive X-ray (EDX) analysis in the different samples are in accordance (within 1-2 wt.%) with their nominal composition. The structure of the milled powders was determined by X-ray diffraction (XRD) using a Bruker D8 diffractometer with Cu K_α radiation.

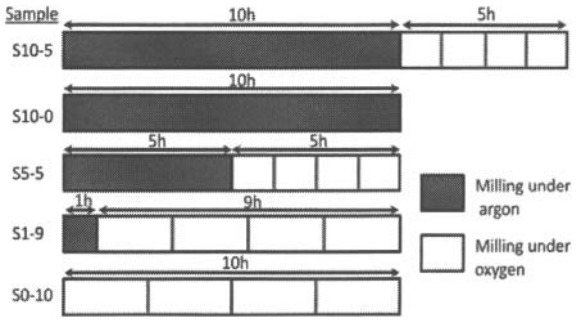

Fig. 1. Schematic representation of the Cu-Ni-Fe-O powders synthesis procedure

The milled powders were consolidated into a 5 mm thick disc electrode. First, the as-milled powders were sieved and particles with a size < 75 μm were selected. They were heated from room temperature to 1000 °C under argon. The resulting thermally softened powder was then cold-pressed at 18 T/cm^2 and sintered at 1100°C under argon for 2 h. The porosity of the consolidated samples was <10%. Their structure was determined by XRD.

Thermogravimetric analyses (TGA) were performed using a Thermax 500 equipment. The consolidated samples were heated from room temperature to 700°C at 10°C min^{-1} under Ar-20%O_2 with a flow rate of 240 cc min^{-1}. The mass variation of the samples was recorded for 5 h. The nature of the oxides formed during these oxidation tests was determined by XRD.

Electrolyses were performed at 700°C under argon atmosphere using a two-electrode configuration cell controlled by a VMP3 Multichannel Potentiostat/Galvanostat (BioLogic Instruments). The electrochemical reactor contains three electrochemical cells and thus, three electrolysis tests can be conducted in parallel. More details on the cell geometry and electrode arrangement are presented elsewhere **[9]**. The geometric surface area of the anode immersed in the electrolyte was ~4 cm^2. The counter electrode was a graphite rod (~13 cm^2 immersed in the electrolyte). The anode-cathode distance was 2.3 cm. The crucibles containing the electrolyte were made of sintered alumina. The electrolyte composition was 50 wt.% AlF_3-45 wt.% KF-5 wt.% Al_2O_3. No alumina was added during the electrolysis since its consumption is assumed to be compensated by the dissolution of the alumina crucible. Electrolyses were performed at an anode current density of 0.5 A cm^{-2} for 20 h. Before measurement, the anode was suspended above the electrolyte for 30 min and then immersed in the electrolyte at open circuit conditions for 10 min. The composition and structure of the oxide layers formed on the anode during Al electrolysis were determined by EDX and XRD analyses after polishing the electrode for different times in order to reveal the successive oxide layers. The surface and cross section of the electrodes were observed by scanning electron microscopy (SEM). The purity of the produced aluminum was determined after 20 h of electrolysis by measuring its Cu contamination determined by neutron activation. The Ni and Fe concentrations could not be used due to an uncontrolled Ni and Fe contamination coming from the corrosion of the Inconel 718 rod used to connect the electrode. However, they would be expected to vary similarly as the Cu levels.

Results and discussion

Structure of the as-milled and consolidated powders.

Figure 2A shows the XRD patterns of the different as-milled powders. All exhibit only one series of peaks which corresponds to a face-centered-cubic (fcc) phase (γ-phase) attributed to a solid solution of Cu(Ni,Fe) or Cu(Ni,Fe,O). Because of its low amount (2.3 wt.%), the addition of oxygen does not induce significant variation of the lattice parameter of the γ-phase (calculated from the (111) peak position) as shown in **Table 1**. After the powder consolidation treatment **(Fig. 2B),** a decrease of the full width at half maximum (FWHM) of the diffraction peaks is observed due to grain growth and strain release. On the basis of Williamson-Hall plots (not shown), the lattice strain is ~0 % and the crystallite size is ~35 nm for the consolidated samples compared to ~0.15% and ~15 nm before consolidation. A very small additional peak is perceptible at ~35° for the consolidated S0-10 and S1-9 samples, which may be attributed to the formation of Fe_2O_3 from O_2 and unalloyed Fe atoms. The fact that the Fe_2O_3 peak is not discernible for the S5-5 and S10-5 samples may indicate that Fe_2O_3 is not formed from the γ-phase. However, this is in contradiction with our recent work showing the formation of Fe_2O_3 inclusions in $Cu_{65}Ni_{20}Fe_{15}$ alloys milled with various amounts of oxygen **[10]**. Actually, the fact that Fe_2O_3 diffraction peaks are not observable for the S5-5 and S10-5 samples in **Fig. 2B** may be due to the finer dispersion of the Fe_2O_3 inclusions in these materials. In other words, the formation of small Fe_2O_3 aggregates in the Cu-Ni-Fe alloy would be more favourable when formed from O and Fe atoms dissolved in the γ-phase (case of S5-5 and S10-5) than from O_2 and unalloyed Fe atoms (case of S0-10 and S1-9). Transmission electron microscopy (TEM) analyses should be done to confirm this issue. As shown in **Table 1**, the consolidation procedure induces a slight decrease of the γ-phase lattice parameter. This could be attributed to the decrease of the Fe content of the γ-phase due to the formation of Fe_2O_3 as confirmed elsewhere **[10]**.

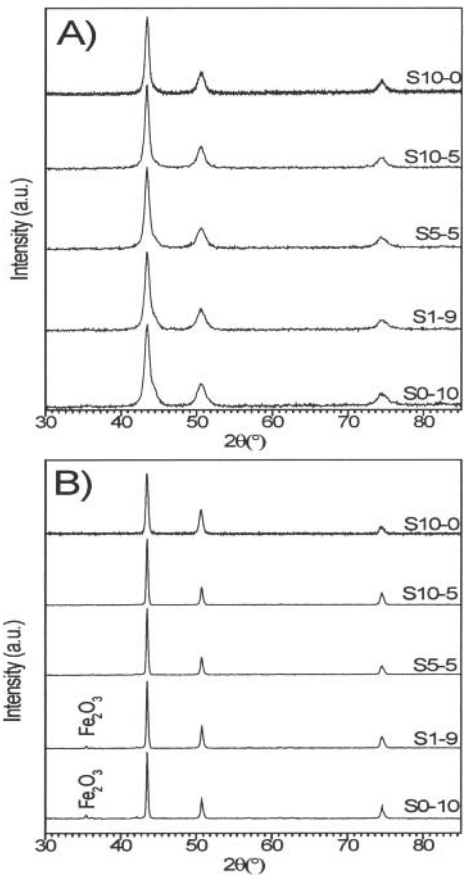

Fig. 2. XRD patterns of the as-milled (A) and consolidated (B) Cu-Ni-Fe-(O) powders.

Table 1. Lattice parameter (Å) of the γ-phase in the as-milled and consolidated samples

	γ-phase lattice parameter (Å)				
Sample	**S0-10**	**S1-9**	**S5-5**	**S10-5**	**S10-0**
As-milled	3.606	3.607	3.606	3.609	3.608
Consolidated	3.603	3.602	3.603	3.603	3.605

High-temperature oxidation behavior

Figure 3 shows the TGA curves for the different consolidated materials. For the sample milled under Ar only (S10-0), a very fast increase in the mass is observed during the two first hours of oxidation, which is attributed to the formation of CuO as confirmed by XRD analysis (not shown). The oxidation rate slows down for t > 2 h due to the formation of $NiFe_2O_4$ acting as a barrier to the copper flux at the oxide-alloy interface [7]. After 5 h of oxidation, the mass gain reaches 4.2 %. For all the samples milled under O_2, the mass gain related to the formation of CuO during the first hours of oxidation is much lower than observed with the S10-0 sample. Moreover, the total mass gain decreases as the pre-milling time under Ar increases. Indeed, the mass gain after 5 h of oxidation is only 0.4 % for the S10-5 sample compared 0.6, 1.0 and 1.2 % for the S5-5, S1-9 and S0-10 samples, respectively. A possible explanation is that the presence of finely dispersed Fe_2O_3 inclusions in the samples milled under O_2 favors the rapid formation of $NiFe_2O_4$ from NiO + Fe_2O_3 during their high-temperature oxidation, thanks to the diminution of the average distance between each compounds. The assumed finer distribution of the Fe_2O_3 inclusions as the pre-milling step under argon increases may accelerate the formation of $NiFe_2O_4$, resulting in a lower oxidation rate as shown in **Fig. 3**.

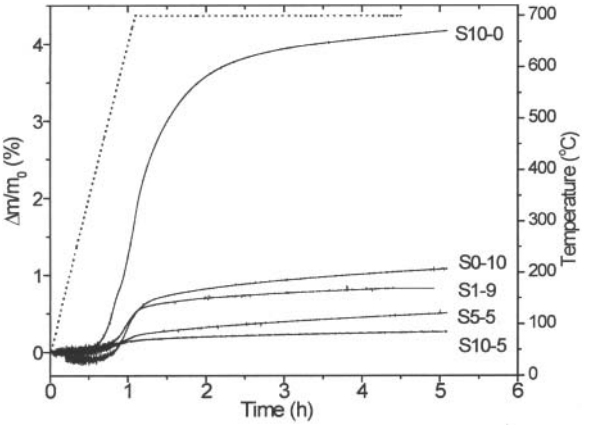

Fig. 3. Variation of the mass gain and temperature with respect to the oxidation time for the consolidated Cu-Ni-Fe-(O) powders.

The XRD patterns of the samples after the oxidation test (**Fig. 4**) confirm the formation of CuO, NiO, FeO and $NiFe_2O_4$ in all cases. However, a comparison of the peak intensity of these oxide phases between the different samples shows that the amounts of CuO and FeO are lower for the S10-5 sample than for the other samples. Moreover, the diffraction peak of the γ-phase observed at ~44° is more intense, indicating that the oxide scale is thinner on the S10-5 sample.

Inert anode behavior

The samples displaying the highest (S10-5) and lowest (S10-0) oxidation resistances on the basis of the previous TGA measurements were evaluated as inert anodes in low-temperature (700°C) KF-AlF_3 electrolyte at I_{anode}= 0.5A cm^{-2}. As shown in **Fig. 5**, both electrodes show a rather similar behavior during the 20 h of electrolysis with a cell voltage around 4-4.5 V. However, the cell voltage with the S10-5 anode is more stable with a variation of *ca.* 0.2 V during the 20 h of electrolysis compared to *ca.* 0.6 V with the S10-0 anode.

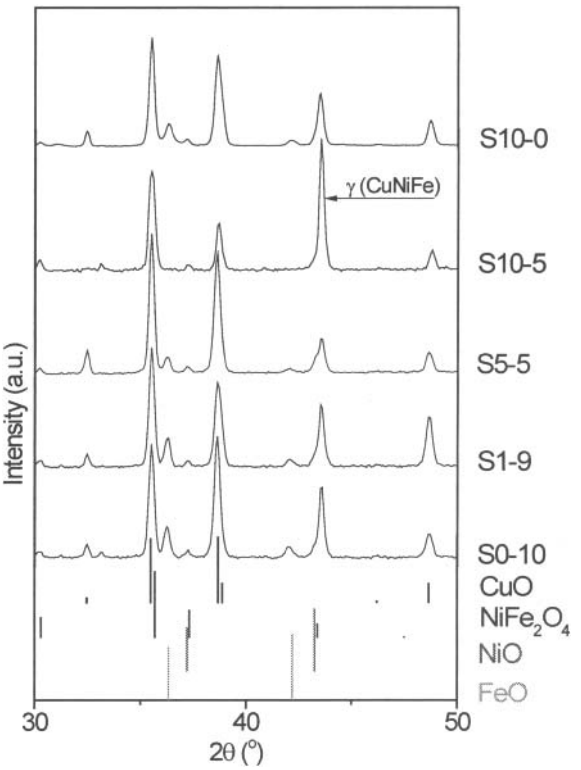

Fig. 4. XRD patterns of the consolidated Cu-Ni-Fe-(O) powders after oxidation for 5 h at 700°C under Ar:O2 (80:20).

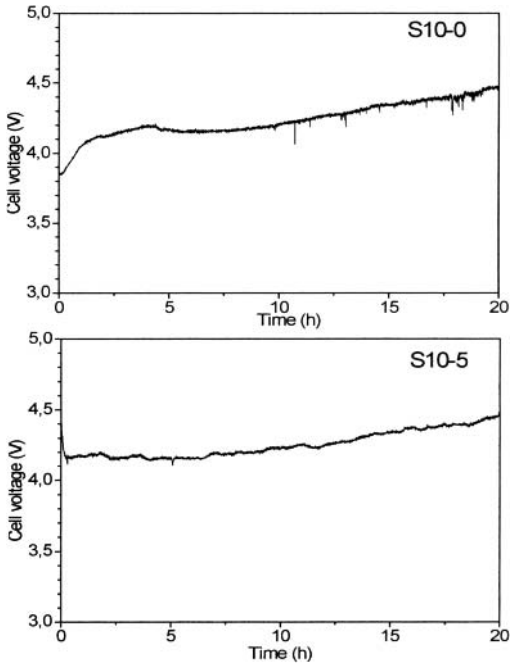

Fig.5. Cell voltage vs. electrolysis time at I_{anode} =0.5 A/cm^2 in KF-AlF_3 (700°C) electrolyte with the S10-0 and S10-5 anodes.

Figures 6A and 6B show the SEM cross-section images of the S10-0 and S10-5 anodes after 20 h of electrolysis, respectively. In both cases, the surface scale is composed of three main layers but their thickness and nature (determined from EDX and XRD analyses recorded after polishing the electrodes for different times, not shown) depend on the electrode composition. At the S10-0 anode (**Fig. 6A**), the surface scale appears dense with a total thickness of ~350μm. The outermost layer is a ~200 μm thick Cu_2O-rich scale containing NiO and FeO_x inclusions. The intermediate layer (~100 μm in thickness) consists of a mixture of Cu_2O and $NiFe_2O_4$ resulting from the outward diffusion of Cu in Cu oxides and the internal oxidation of Fe and Ni with the subsequent formation of $NiFe_2O_4$ as discussed in previous works **[7,8]**. Near the bulk alloy, a non-continuous layer of FeF_2 (~50 μm in thickness) is observed, which may be preferentially formed when the anode was maintained above the electrolyte for 30 min and during the first minutes of electrolysis as suggested in **[8]**. For the S10-5 anode, the surface scale is thinner with a total thickness of ~150 μm. The outermost layer (~50 μm thick) is composed of $NiFe_2O_4$ with Cu_2O as a minor constituent. Underneath, a layer (~50 μm thick) containing Cu_2O as major constituent and some $NiFe_2O_4$ is present. Finally, the inner layer (~50 μm thick) is constituted of FeF_2 inclusions inside the alloy matrix as observed for the S10-0 anode. The fact that the outermost layer is thinner and much poorer in Cu_2O on the S10-5 anode than on the S10-0 anode confirms that the outward diffusion of Cu in Cu oxides is significantly slowed down. As discussed before, this is attributed to the more favorable formation of $NiFe_2O_4$ (in accordance with the observation of a $NiFe_2O_4$-rich outermost layer) due to the presence of finely dispersed Fe_2O_3 precipitates in the Cu-Ni-Fe matrix, acting as nucleation sites for the formation of $NiFe_2O_4$.

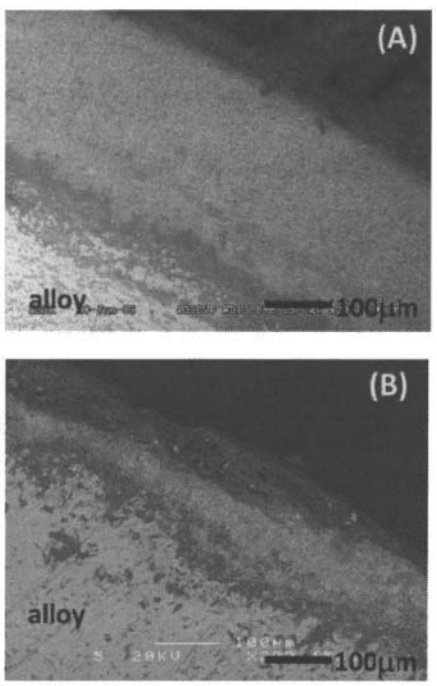

Fig.5. SEM cross section micrographs of the S10-0 (A) and S10-5 (B) anodes after 20h of electrolysis in low-temperature (700°C) KF-AlF_3 electrolyte.

The Cu contamination level in the produced aluminum is lower with the S10-5 anode (0.2 wt.%) than with the S10-0 anode (0.4 wt.%). This confirms the better corrosion resistance of the S10-5 electrode as argued previously. This result is very promising considering that the small scale and short term electrolysis tests tend to give higher impurities in the produced Al than during industrial electrolysis.

Conclusion

This work has shown the efficiency of the ball milling technique performed under O_2 atmosphere for inducing the formation of Fe_2O_3 inclusions in Cu-Ni-Fe alloy during the subsequent powder consolidation treatment. These well-dispersed Fe_2O_3 precipitates are assumed to favor the rapid formation of a $NiFe_2O_4$-rich layer on the anode surface during Al electrolysis in low-temperature (700°C) KF-AlF_3 electrolyte, resulting in an improvement of the anode corrosion resistance.

Acknowledgment

The authors thank the "Fonds de Recherche du Québec - Nature et Technologies" for supporting this work.

References

[1] T.R. Beck, R.J. Brooks *"Non-consumable anode and lining for aluminium electrolytic reduction cell"* US patent 5,284,562 (1994).

[2] T.R. Beck, *"A non-consumable metal anode for production of aluminum with low-temperature fluoride melts"* Light Metals 1995 (TMS, Warrendale, Pa), 355-360.

[3] H.X. Li, X.J. Hao, G. Zhao, S.M. Hao, *"Characteristics of the continuous coarsening and discontinuous coarsening of spinodally decomposed Cu-Ni-Fe alloy"* J. Mater. Sci. , 36 (2001) 779– 784.

[4] T.R. Beck, C.M. MacRae, N.C. Wilson, *"Metal anode performance in low-temperature electrolytes for aluminum production"*, Metall. Mat. Trans. B, 42 (2011) 807-813

[5] S.C. Bergsma, C.W. Brown, D.R. Bradford, R.J. Barnet, M. B. Mezner, *"Cu-Ni-Fe anode for use in aluminum producing electrolytic cell"*, US Patent 7,7077,945 (2006).

[6] B. Assouli, M. Pedron, S. Helle, A. Carrere, D. Guay, L. Roué, *"Mechanically alloyed Cu-Ni-Fe based materials as inert anode for aluminum production"*, Light Metals 2009 (TMS, Warrendale, Pa), 1141-1144.

[7] S. Helle, M. Pedron, B. Assouli, B. Davis, D. Guay, L. Roué, *"Structure and high-temperature oxidation behavior of Cu-Ni-Fe based alloys prepared by high-energy ball milling for application as inert anodes for aluminum electrolysis"* Corros. Sci., 52 (2010) 3348-3355.

[8] S. Helle, B. Brodu, B. Davis, D. Guay, L. Roué, *"Influence of the iron content in Cu-Ni based inert anodes on their corrosion resistance for aluminium electrolysis"*, Corros. Sci., 53 (2011) 3248-3253.

[9] S. Helle, B. Davis, D. Guay, L. Roué, *"Electrolytic production of aluminum using mechanically alloyed Cu-Al-Ni-Fe based materials as inert anodes"*, J. Electrochem. Soc., 157 (2010) E173-179.

[10] S. Helle, B. Davis, D. Guay, L. Roué, *"Mechanically alloyed Cu-Al-Ni-O based materials as* oxygen-evolving anodes for aluminum electrolysis", J. Electrochem. Soc., submitted.